CD and MCD Spectroscopic Studies of the Two Dps Miniferritin Proteins from Bacillus anthracis: Role of O−2 and H2O2 Substrates in Reactivity of the Diiron Catalytic Centers

ARTICLE *in* BIOCHEMISTRY · OCTOBER 2010

Impact Factor: 3.02 · DOI: 10.1021/bi101346c · Source: PubMed

Published in final edited form as:
Biochemistry. 2010 December 14; 49(49): 10516–10525. doi:10.1021/bi101346c.

CD AND MCD SPECTROSCOPIC STUDIES OF THE TWO DPS MINI-FERRITIN PROTEINS FROM *B. ANTHRACIS:* ROLE OF O_2 AND H_2O_2 SUBSTRATES IN REACTIVITY OF THE DI-IRON CATALYTIC CENTERS

Jennifer K. Schwartz[‡], **Xiaofeng S. Liu**[§], **Takehiko Tosha**[§], **Adrienne Diebold**[‡], **Elizabeth C. Theil**[§,‖,*], and **Edward I. Solomon**[‡,*]

[‡]Department of Chemistry, Stanford University, 333 Campus Drive, Stanford, California 94305

[§]Council for BioIron at CHORI (Children's Hospital Oakland Research Institute), 747 52nd Street, Oakland, California 94609

[‖]Department of Nutritional Sciences and Molecular Toxicology, University of California-Berkeley, Morgan Hall, Berkeley, CA 94720-3104

Abstract

DNA Protection during Starvation (Dps) proteins are mini-ferritins found in bacteria and archaea that provide protection from uncontrolled Fe(II)/O radical chemistry; thus the catalytic sites are targets for antibiotics against pathogens, such as anthrax. Ferritin protein cages synthesize ferric oxymineral from Fe(II) and O_2/H_2O_2, which accumulates in the large central cavity; for Dps, H_2O_2, is the more common Fe(II) oxidant contrasting with eukaryotic maxi-ferritins that often prefer dioxygen. To better understand the differences in the catalytic sites of maxi versus mini-ferritins, we used a combination of NIR circular dichroism (CD), magnetic circular dichroism (MCD), and variable-temperature, variable-field MCD (VTVH MCD) to study Fe(II) binding to the catalytic sites of the two *B. anthracis* mini-ferritins; one in which two Fe(II) react with O_2 exclusively (Dps1) and a second in which both O_2 or H_2O_2 can react with two Fe(II) (Dps2). Both result in the formation of iron oxy-biomineral. The data show: a single 5 or 6-coordinate Fe(II) in the absence of oxidant; Fe(II) binding to Dps2 is 30 × more stable than Dps1; and the lower limit of K_d for binding a second Fe(II), in the absence of oxidant, is 2–3 orders of magnitude weaker than for the binding of the single Fe(II). The data fit an equilibrium model where binding of oxidant facilitates formation of the catalytic site, in sharp contrast to eukaryotic M-ferritins where the binuclear Fe(II) centers are preformed before binding of O_2. The two different binding sequences illustrate the mechanistic range possible for catalytic sites of the family of ferritins.

DNA Protection during Starvation (Dps) proteins, also known as mini-ferritins, are 12-monomer spherical proteins capable of storing iron mineral and thus are part of the ferritin super-family (1–4). Unlike maxi (24-monomer) ferritins, Dps proteins have been shown to bind and protect DNA from oxidation (2–4). The paired Dps proteins in *Bacillus anthracis*

[*]To whom correspondence should be addressed: Elizabeth C. Theil etheil@chori.org; phone: 510-450-7670; fax: 510-597-7131; and Edward I. Solomon, edward.solomon@stanford.edu; phone: 650-723-4694; fax: 650-725-0259.

Supporting Information Available

CD spectra showing effect of temperature on Dps1 transitions; MCD spectra of Dps1 overlaid with Fe(II) control spectrum, and MCD spectrum with control subtracted; Apparent initial rates of Fe^{2+} oxidation in Dps1 & 2 scaled to overlay with the calculated concentration of binuclear Fe(II) active sites occupied at a given Fe^{2+}/Dps2 ratio using fixed K_{D1} and varied K_{D2} values. This material is available free of charge via the Internet at http://pubs.acs.org.

(Dps1 and Dps2), which share ~60% sequence homology(3), confer greatest protection when both are present. Dps proteins in pathogens, such as those from *B. anthracis*, are of particular interest as better knowledge of how these proteins protect pathogens from oxidative damage can provide insight into whether Dps proteins could be possible drug targets against anthrax and other bacterial diseases. Unfortunately only a small amount of information is available about Fe(II) protein interactions in the Dps proteins (5). Crystal structures of both *B. anthracis* proteins have been solved (6), and show significant differences between the maxi and mini-ferritin ferroxidase sites. In contrast to diiron sites in the 24 subunit ferritins, the active sites in the Dps proteins are located between subunits rather than within a 4-α helix bundle, with few exceptions (5,7). Moreover, there appear to be only enough ligands to form one available binding site for an Fe(II) at the proposed active site, despite a stoichiometric ratio of 2Fe(II) required per site being computed from the kinetics data (3). Both Dps1 and 2 show a single iron atom with tetrahedral coordination bound by histidine, aspartate, and glutamate ligands plus one water molecule (Figure 1) (8). Several additional water molecules plus a second histidine are nearby, suggesting a potential binding location for the second iron and a few other crystal structures have been obtained for different Dps or Dps-like proteins, with varying numbers of iron atoms present (2,7). For both Dps1 and 2, rates of Fe(II) oxidation with O_2 are about 10-fold slower than those of the maxi-ferritins and an intermediate peroxo species is not observed (3). In Dps2, however, the rate of reactivity between Fe(II) and H_2O_2 is about 3-fold faster than its rate of O_2 reactivity, and an intermediate with an absorption feature at 650nm, similar to the peroxo species in maxi ferritin, is observed. Dps1 shows no reactivity with H_2O_2 and in fact has been shown to inhibit protein independent Fe(II) + H_2O_2 reactions (3). These data, along with sequence similarities between other Dps proteins, suggest that the function of Dps1 is iron sequestration while the Dps2 carries out H_2O_2 destruction, accounting for why the pair confers the most DNA protection when both are present. Because these proteins present an oxidant continuum from hydrogen peroxide to dioxygen and function in both anaerobic and aerobic environments, understanding the structure of the metal binding sites in mini-ferritins may provide insights on the evolution of the dioxygen-dependent active sites present in ferritins of many contemporary organisms.

To determine the Fe(II) binding properties of this paired set of Dps proteins in solution and elucidate the relationship between mini and maxi-ferritins, a methodology utilizing Circular Dichroism (CD), Magnetic CD (MCD) and Variable Temperature, Variable Field (VTVH) MCD was used to probe the geometric and electronic structural features of the Fe(II) substrate sites. This methodology has been developed and applied to a number of bi-ferrous cofactor sites, in which Fe(II) remains coordinated to the active site throughout the reaction (9), and has recently been used to study the ferroxidase site in a maxi ferritin, in which the irons are substrates that are released from the site after reaction (10). Here, CD/MCD titrations are used to provide binding constants for each of the substrate sites in Dps1 and Dps2, and find that only a single Fe(II) binds to each site under the anaerobic conditions of the experiment. This allows us to develop an equilibrium model of Fe(II) binding where O_2 or H_2O_2 are required for formation of the binuclear Fe(II) active site. The significant differences in binding and structure of these substrate sites are then discussed in terms of their reactivity with O_2 and H_2O_2 and the possible relationships to distinct physiological functions of maxi- and mini-ferritins.

2. Materials and Methods

2.1 Sample Preparation

MOPS buffer (Sigma), NaCl (EMD Chemicals, Inc.), deuterium oxide (99.9 atom % D, Aldrich), sodium dithionite (Sigma), ferrous sulfate heptahydrate (Baker), and glycerol-d_6 (98% D, Cambridge Isotope Laboratories) were commercially purchased, and used as

obtained. Before use in an inert atmosphere, D_2O was degassed with 99.9% pure argon, glycerol was degassed by heating under vacuum overnight at 10^{-3} Torr, and solid ferrous sulfate was put under vacuum at 10^{-3} Torr for at least one hour. Fe(II) stock solutions (~60–100 mM depending on protein concentration), used for reconstitution of the apo-protein, were freshly prepared before each experiment by adding anaerobic D_2O to a pre-measured amount of degassed solid ferrous sulfate under nitrogen atmosphere.

Recombinant apo Dps1 and Dps2 proteins from *Bacillus anthracis* were expressed and purified as previously reported (3). The protein buffer solution was then exchanged with a deuterium oxide buffer solution of 100 mM Mops/100 mM NaCl at pD 7.3 until the percentage of D_2O was 99.9% of the solvent. One set of samples was also exchanged into an unsalted buffer solution. Removal of salt was found to have no effect on CD/MCD data. All protein solutions were then concentrated to between ~0.75 – 4 mM per subunit with one catalytic site/subunit (0.0625–0.33 mM protein nanocages), and degassed while on ice by rapidly purging with at least 30 vacuum/argon cycles.

To prepare the CD and MCD samples, incremental amounts of Fe(II) stock solution were added to the anaerobic apo-protein solution, and after incubation for ~10 minutes, CD samples were measured in an anaerobic quartz cuvette, which was cooled to 7°C by a re-circulating water bath. MCD samples were similarly prepared with an additional step of mixing the protein solution with 50–60% (v/v) glycerol-d_6 until homogeneous to create a suitable glass. The protein samples were then injected into the MCD sample cell (a neoprene spacer of 0.3 cm path length compressed between two infrasil quartz disks that are held together between two fitted copper plates) while under an inert atmosphere, and immediately frozen in liquid nitrogen.

2.2 CD and MCD Spectroscopy

CD studies were performed on a JASCO J200D spectropolarimeter operating with a liquid nitrogen-cooled InSb detector in the 600–2000 nm region. Low-temperature MCD and VTVH MCD data were acquired on this spectropolarimeter, modified to accommodate an Oxford Instrument SM4000 7T-superconducting magnet capable of magnetic fields up to 7.0 Tesla and temperatures down to 1.5 K. The depolarization of the protein glass was checked by comparing CD spectra taken with a freshly prepared nickel (+)-tartrate solution placed immediately before, and then after the MCD sample compartment (11). Less than 5% depolarization was observed.

All CD and MCD spectra were baseline corrected by subtracting the apo-protein solution spectrum, or averaging the corresponding positive and negative field spectra at a particular temperature. These spectra were then fit with Gaussian band shapes using a constrained nonlinear least-squares procedure in order to find the minimum number of ligand field transitions required to simultaneously fit both spectra. VTVH MCD data (MCD intensity at a specific wavelength as a function of temperature and applied magnetic field) were fit using a simplex routine that minimizes the χ-squared value. A goodness of fit parameter (χ-squared/number of float parameters) was utilized in the comparison of fit results.

3. Results

3.1 Metal Binding to the Ferroxidase Site and Excited State CD/MCD Spectra

3.1.1 Dps1—Fe(II) binding to the apo-Dps1 protein, the dioxygen selective mini-ferritin, was monitored using Near-IR (NIR) CD and MCD titrations. In CD, one broad band is observed upon addition of Fe(II) (Figure 2, black). This band is slightly perturbed by glycerol, but as temperature decreases, the sign of the low energy transition changes

(Supporting Information, Figure S1). Nearly identical perturbations to the CD are observed upon addition of an alternative glassing agent, sucrose. It is possible that because the active site is located between subunits (6), as opposed to within the 4-α helix bundle of the subunit as in maxi ferritins (12) and most other diiron enzymes (13–17), the site is more susceptible to conformational variation. As this perturbation does not change the energy of the transitions, it does not appear to affect the actual coordination environment of the iron center.

Titration of Dps1 with Fe(II) under anaerobic conditions leads to saturation of this CD signal at approximately 1.2 Fe(II) per Dps subunit (where 12 subunits make up a Dps protein cage), as shown in figure 2A. This band can be resolved into two transitions at ~8000 and 10000 cm^{-1} upon simultaneous peak fitting with low temperature CD and MCD spectra (*vide infra*). These transitions correspond to d →d ligand field transitions of the ferrous site and must derive from Fe(II) sites within the protein, as only chiral iron centers will contribute to the CD spectrum (18). To determine the Fe(II) binding affinity for the protein sites, the CD intensity of each transition (Δε) is plotted against the concentration of Fe(II) (Figure 2C). As the protein and iron concentrations are of the same order of magnitude, binding curves from each data set were fit to equation 1 (19) using Microcal Origin Pro 6.1 (20) to determine the dissociation constant, K_D, and number of Fe(II) binding sites, n:

$$A=\Delta\varepsilon\left(\frac{K_D+n[P_T]+[L_T]\pm\sqrt{(K_D+[P_T]+[L_T])^2-(4n[P_T][L_T])}}{2n[P_T]}\right) \quad (1)$$

where A is the CD intensity at a given wavelength with the corresponding Δε, $[P_T]$ is the total concentration of Dps protein (per subunit), and $[L_T]$ is the total concentration of Fe(II) added. For Dps1 the K_D is determined to be approximately 77 μM for the first Fe(II) binding site (Table 1). The binding curve is best fit with n ~ 0.9 indicating that only one Fe(II) binding site is present (Figure 2C). Each transition is fit with the same parameters, further supporting a single Fe(II) site, which can exhibit at most two LF transitions in the near-IR CD spectrum. Aerobic kinetic studies determined that a 2Fe(II) : $1O_2$ ratio was required for reaction (3), therefore the lack of a second binding site under anaerobic conditions suggested that O_2 might play a role in formation of the active site. To determine if a second Fe(II) binding site with a much weaker affinity could be observed under anaerobic conditions, titrations with lower protein concentrations were performed to increase the ratio of Fe(II) : protein. (Note that protein-bound Fe(II) must be at least ~0.2 – 0.3 mM Fe(II) to observe ligand field transitions within the sensitivity of the CD experiment.) A maximum of 9.5 equivalents of Fe(II) per protein subunit was achieved before protein denaturation, however no additional features were observed in CD. From these conditions it can be determined that if a second Fe(II) binding occurs without dioxygen, its K_D must be greater than ~40,000 μM; i.e. at least two to three orders of magnitude weaker than the first Fe(II), and therefore cannot be observed within the sensitivity of this experiment.

From MCD titrations it is observed that, as in CD, there are two transitions present which grow together upon addition of Fe(II): a positive band at ~7800 cm^{-1} and a small negative band at ~11000 cm^{-1} (Figure 2B). At Fe(II) concentrations greater than 1 equivalent per subunit, a large positive feature between 8000 and 11,000cm^{-1} begins to dominate the spectrum (Figure 2B, green). While only transitions from protein-bound Fe(II) will be observed in CD, Fe(II) in a MOPS buffer solution is 6 coordinate and will be associated with two large transitions at 9200 and 10,785 cm^{-1} in MCD that can obscure Fe(II) active site transitions in this region (Supporting Information, Figure S2A,B). Therefore, to determine if

these new MCD features are associated with the binding of a second Fe(II) center to Dps1 or simply are from excess Fe(II) in solution, the contribution of excess Fe(II) to the MCD spectrum was calculated from the K_D value determined above and subtracted from each MCD spectrum (Supporting Information, Figure S2B,C). Although the first iron binding site has a fairly high affinity for Fe(II), there is a 5–15% contribution from Fe(II) in MOPS solution to each of the MCD spectra. Figure S2C, in the supporting information, shows the spectra from the MCD titrations, with contributions from ferrous iron in solution removed, indicating that above 1 equivalent of Fe(II) per subunit there are no additional MCD features observed that can be attributed to a second Fe(II) binding site in Dps1. Thus both CD and MCD titrations indicate the presence of one Fe(II) center with a high binding affinity in Dps1. A simultaneous peak fit of the CD, low temperature CD, and MCD spectra with excess Fe(II) contributions subtracted confirm that there are two transitions associated with the iron binding site of Dps1: one positive band at 7800 cm^{-1} and one negative band at 10870 cm^{-1} (Figure 3A).

3.1.2 Dps2—The conditions used for Dps 1 were also used to monitor the Fe(II) binding to the ferroxidase sites of Dps2. One broad positive feature is observed in the CD spectrum in the same energy region as in Dps1 (Figure 4A), suggesting that the ferroxidase sites within each Dps protein have similar conformations around the active sites. In Dps2 this band saturates at approximately 1.3 equivalents of Fe(II) per subunit, under anaerobic conditions (Figure 4A). Fitting with equation 1 yields a smaller K_D (~2 μM) and larger n (~1.3) relative to Dps 1 (Table 1), again indicating a single Fe(II) binding site with a higher binding affinity than Dps1. The addition of up to 9 equivalents per subunit did not produce any additional change in CD. In the MCD spectrum, the addition of greater than 1 equivalent per subunit again leads to dominant transitions from the excess Fe(II) in solution (Figure 4B). Subtraction of the excess Fe(II) signal leads to a nearly identical spectrum as that observed with less than 1 equivalent of Fe(II) (Figure 4C, green), again supporting the lack of a second Fe(II) binding to the ferroxidase site in Dps2. From these conditions it can be determined similarly that if a second Fe(II) binding can occur without dioxygen, its K_D must be greater than ~20,000 μM; again more than two orders of magnitude weaker than the first Fe(II) binding site. Simultaneous peak fitting of the CD, low temperature CD, and MCD spectra for the single iron binding site in Dps2 yields two positive transitions at 8300 and 10300 cm^{-1} (Figure 3B). The splitting between these transitions is ~1000 cm^{-1} less than that observed for Dps1 and the higher energy transition is now positive in contrast to the negative band observed in Dps1 (Figure 3A), suggesting a difference in coordination numbers or geometries between these two Dps proteins.

3.2 VTVH MCD: Ground state analysis

Increasing field or decreasing temperature leads to an increase, and eventual saturation, of the MCD intensity of both transitions, indicating that each is dominated by an MCD C-term mechanism associated with a paramagnetic doublet ground-state. Different rates of temperature and field saturation were observed at different energies, and can reflect different Fe(II) centers or different polarizations associated with each transition (18). Therefore, variable temperature, variable field (VTVH) MCD data were collected at energies where there was minimal overlap of resolved band intensities (Figure 3, arrows). In Dps1, VTVH MCD data were obtained at 7185 and 11,000 cm^{-1}, and are shown in Figure 5, where the relative intensities of the VTVH MCD curves are plotted against βH/2kT. The offset of the low temperature isotherms from those at higher temperatures is characteristic of low lying excited states and rhombic zero-field splitting (ZFS) of non-Kramers doublet ground states (21). Ground state parameters for a non-Kramers system can be obtained through doublet fitting of the VTVH MCD intensity (Figure 5–6) using equation 2 (18,22–24):

$$\Delta\varepsilon = \sum_i \left[(A_{sat\,\lim})_i \left(\int_0^{\frac{\pi}{2}} \frac{\cos^2\theta \sin\theta}{\Gamma_i} g_{\|i}\beta H\alpha_i d\theta - \sqrt{2}\frac{M_z}{M_{xy}} \int_0^{\frac{\pi}{2}} \frac{\sin^3\theta}{\Gamma_i} g_{\perp i}\beta H\alpha_i d\theta \right) + B_i H\gamma_i \right] \quad (2)$$

where

$$\Gamma_i = \sqrt{\delta_i^2 + (g_{\|i}\beta H\cos\theta)^2 + (g_{\perp i}\beta H\sin\theta)^2}$$

$$\alpha_i = \frac{e^{-(E_i-\Gamma_i/2)/kT} - e^{-(E_i+\Gamma_i/2)/kT}}{\sum_j e^{-(E_j-\Gamma_j/2)/kT} + e^{-(E_j+\Gamma_j/2)/kT}}$$

$$\gamma_i = \frac{e^{-(E_i-\delta_i/2)/kT} + e^{-(E_i+\delta_i/2)/kT}}{\sum_j e^{-(E_j-\beta_j/2)/kT} + e^{-(E_j+\delta_j/2)/kT}}$$

This equation allows for the contribution of C-term intensity, $(A_{satlim})_i$, the rhombic ZFS for a non-Kramers doublet, δ_i, the effects of a linear B-term from field induced mixing between states, B_i, and the presence of thermally excited sublevels of the ground state. E_i is the energy of the i^{th} excited state, and the energy of the ground state is defined as zero. The Boltzmann population over all states has been included in both the *C*- term and the *B*- term intensities as the factors α_i and γ_i, respectively. *H* is the applied magnetic field, *k* the Boltzmann constant, M_z and M_{xy} are the transition dipole moments for the directions indicated, and $g_{\|i}$ and $g_{\perp i}$ are the Zeeman splitting parameters of the *i*th doublet. Each VTVH MCD data set for Dps1 was fit with equation 2 by exploring all possible $g_\|$ values that could be associated with each of the possible ground states for a high spin Fe(II) dimer and monomer system. Good fits for each set were independently achieved with $g_{\|0}$~9.1 ± 0.2 and δ_0 ~ 3.7 ± 0.2 cm^{-1}, indicative of a M_s = ±2 ground state. Differences in the $(A_{satlim})_0$ and B_0 parameters account for the different nesting behaviors of each transition.

An M_s = ±2 ground state could derive from a mononuclear or an exchange coupled binuclear non-heme iron site. In order to independently evaluate the later possibility, a full spin Hamiltonian analysis for an exchange coupled dimer system was performed as previously described (10), to determine if any exchange coupling between Fe(II) centers is reflected by the data. An exchange constant of J ~ 0 cm^{-1} was found, again supporting a single Fe(II) site with no interaction with a second Fe(II) under anaerobic Fe(II) loading conditions. Thus a full analysis for a mononuclear non-heme iron site was carried out. This analysis determined that the single Fe(II) center for Dps1 is best described by a Δ = −300 ± 100 cm^{-1} with $|V/2\Delta| \approx 0.20 \pm 0.02$ for the dπ orbital splittings where Δ is the energy difference between the d_{xy} and $d_{xz,yz}$ orbitals and *V* defines the splitting of the *xz* and *yz* orbitals (22). The positive and negative bands observed in CD/MCD split by slightly greater than 3000 cm^{-1} are generally characteristic of a distorted square pyramidal site, however the larger $g_\|$ and δ ground state parameters and therefore small Δ, suggest that a 6 coordinate site with a weak axial water ligand may also be possible (25).

The same analysis was carried out for the VTVH MCD data obtained at 7800 and 11,000 cm^{-1} for Dps2. It was again found that no exchange coupling is present, and the ground state is well described by $g_\| = 9.0 \pm 0.2$ and $\delta = 3.9 \pm 0.2$ cm^{-1}. These ground state parameters give Δ = −250 ± 100 cm^{-1} with $|V/2\Delta| \approx 0.19 \pm 0.01$. The combination of these ground state parameters and the two positive transitions at 8300 and 10300 cm^{-1}, which are split by only 2000 cm^{-1}, indicate that the site in Dps2 is also 6 coordinate.

3.3 Speciation curves and correlation to reactivity

Ground state analysis of the VTVH MCD data for both Dps1 and Dps2 were consistent with the excited state titration data, both indicating that only one Fe site has been loaded under these experimental conditions. In section 3.1 it was determined that in Dps1, the dissociation constant for a second Fe(II) binding must be greater than ~40,000 μM; and the dissociation constant for a second Fe(II) binding in Dps2 must be greater than ~20,000 μM; each more than two orders of magnitude weaker than the first Fe(II) binding site. Previous kinetics data (3) clearly demonstrated that the rate of iron oxidation in both Dps proteins was dependent on the concentration of Fe(II) present and that there was a significant increase in the rate of oxidation at approximately 24Fe(II)/protein dodecamer. This distinct increase was attributed to the filling of all 12 putative di-iron sites within a Dps molecule, and the further increase in rate caused by additional oxidation at the now available mineral core or other types of protein bound sites (3). In order assess this model, the new binding constants in Table 1 were used to calculate a set of speciation curves that determine the concentrations of mononuclear sites versus binuclear sites available to react.

The system was modeled with the following set of equilibria

$$P_f + Fe_f \overset{\frac{1}{K_{D1}}}{\longleftrightarrow} P_1 + Fe_f \overset{\frac{1}{K_{D2}}}{\longleftrightarrow} P_2 + Fe_f \tag{3}$$

where Fe_f is the free (unbound) Fe(II) in solution, P_f is the concentration of unbound protein monomers, P_1 is the concentration of monomers with a single iron site loaded, and P_2 is the concentration of monomers with diiron sites loaded. A system of four equations was defined where Fe_T is the known total Fe(II) concentration available,

$$[Fe_T] = [Fe_f] + [P_1] + 2^*[P_2] \tag{4}$$

P_T is the known total protein concentration available,

$$[P_T] = [P_f] + [P_1] + [P_2] \tag{5}$$

and the dissociation constants are equal to the following ratios

$$K_{D1} = \frac{[P_f][Fe_f]}{[P_1]} \tag{6}$$

$$K_{D2} = \frac{[P_1][Fe_f]}{[P_2]} \tag{7}$$

Equations 3 through 7 were solved numerically to determine the concentrations of mononuclear and binuclear iron sites available at a given Fe to protein ratio based on the equilibrium model proposed in equation 3. Speciation curves from one of these calculations are shown in Figure 7, where $[P_f]$, $[P_1]$, $[P_2]$, & $[Fe_f]$ are plotted as a function of $[Fe_T] / [P_T]$. The total protein concentration was fixed at 240 μM while total Fe(II) concentration was varied from 0 to 1M (~4200 Fe^{2+}/Dps). The dissociation constant, K_{D1} was fixed at the experimentally determined (by CD titration) value of 77 μM and K_{D2} was fixed at 40,000 μM, the lower limit determined for the second iron binding in Dps1 (Table 1). It is clear that

the concentration of mononuclear sites rapidly increases due to the strong binding of the first iron, however the experimentally determined maximum for the second Fe(II) binding constant is much weaker, and therefore formation of the full binuclear site is very limited, even at higher concentrations of Fe(II). At approximately two equivalents of Fe(II), essentially all the active sites have at least one iron bound however only 5% of the active sites have actually formed diiron sites. An overlay of the calculated concentration of available diiron sites with the previously measured apparent velocities at varying Fe(II)/Dps ratios (Figure 8) indeed shows that the initially low reactivity can be correlated with the low availability of diiron sites. However, if the concentration of binuclear Fe(II) active sites is calculated using a K_{D1} of 77 μM and K_{D2} of 40,000 μM, the minimum possible K_{D2} allowed by our experimental binding constants under anaerobic conditions as determined by the CD titration in Figure 2, it is clear that the concentration of diiron sites does not increase as quickly as the apparent velocity of Dps1 (red curve, Figure 8a, supporting information Figure S3). This suggests that the addition of oxygen (or hydrogen peroxide in the case of Dps2) to the protein solution must assist in the formation of the diiron site by increasing the affinity for one or both irons. Lowering K_{D1} was found to decrease the number of P2 sites available at 2 equivalents and thus provides a worse fit. Lowering K_{D2} to 15,000 μM, however, produces a sharper increase in the availability of diiron sites, correlating well with the increase in reactivity (blue curve, Figure 8a). This suggests a new equilibrium model for this system, in which O_2 must assist in the binding of the second iron:

$$P_f + Fe_f \overset{\frac{1}{K_{D1}}}{\longleftrightarrow} P_1 + Fe_f + O_2 \overset{\frac{1}{K_{D2}}}{\longleftrightarrow} P_2 + Fe_f \quad (8)$$

The data for the O_2 reaction of Dps2 show a similar effect. An overlay of the measured apparent velocities of Dps2 (Figure 8b, supporting information Figure S4) versus the concentrations of available diiron sites calculated with K_{D1} of 2.1 μM and K_{D2} of 20,000 μM (Table 1) shows that the affinity for the second Fe(II) must increase (red curve) so that when the second dissociation constant is lowered to approximately 15,000 μM a reasonable fit is achieved (black curve). Thus with both mini-ferritins, the initially low reactivity with dioxygen can be correlated with the low availability of diiron sites. The availability of diiron sites is shown to increase in the presence of O_2, which assists in the binding of the second iron.

In Dps 2, the aerobic reaction with H_2O_2 was 3-fold faster than with O_2 alone, and the anaerobic reaction with H_2O_2 was 5-fold faster (3). Fitting of the apparent velocities for the reaction of Dps2 with H_2O_2 thus requires an even higher affinity for the second iron binding at the Dps2 active site. In contrast, Dps1 showed no reactivity with H_2O_2, with or without oxygen; in fact Dps1 was found to inhibit the solution reaction between Fe(II) and H_2O_2, independent of Fe concentration. This can be accounted for by the high affinity of the first iron binding site, which shows that there would be little free iron in solution (<100 μM) available for such a reaction below the addition of 1 equivalent of iron (Figure 7).

4. Discussion

In the ferritin super-family, protein based Fe/O chemistry in 24-subunit (maxi) and 12 subunit (mini) ferritins differs in at least two significant ways. First, in maxi ferritins the primary oxidant used at the di-iron active site tends to be dioxygen, whereas either dioxygen or hydrogen peroxide can be used in the mini-ferritins, with hydrogen peroxide being the more common (5,26). Secondly, although Fe(II) reaches the catalytic sites in both maxi-and mini-ferritin through pores formed at the junction of three subunits (26,27), the location of the catalytic sites is quite different. In maxi-ferritins, the Fe(II) substrates bind at an active

site buried deep within the four helix bundles of each subunit, which also contain sites for mineral nucleation among the catalytic diferric-oxo products (28). By contrast, Fe(II) catalytic sites in most mini-ferritins are formed by ligands provided by two subunits across the dimer interface (5,6). Thus the mineral precursors are spatially formed on the protein surface of the mineralization cavity in mini-ferritins making it unlikely that the protein cage contributes to mineral nucleation and accretion, as in maxiferritins. In order to further elucidate differences in the catalytic sites between these two proteins we used excited state CD/MCD titrations and ground state VTVH MCD data to probe the Fe(II) binding at the catalytic sites in two mini-ferritins from *B. anthracis*. From these analyses we have concluded: 1) Only a single Fe(II) binds to the mini-ferritin active sites in the absence of oxidant; 2) Fe(II) binding to Dps2, which uses either O_2 or H_2O_2 as an oxidant is much tighter than for Dps1; 3) The lower limit for K_{D2}, the dissociation constant for the second iron as determined from the CD titration in the absence of oxidant, shows that the binding of this Fe(II) is at least hundreds to thousands of time weaker than binding of the first Fe(II); 4) The O_2 or H_2O_2 substrate is required to drive the formation of the diiron site.

From the excited state CD/MCD titrations and the ground state VTVH MCD analysis it can be concluded that under anaerobic conditions and concentrations of our experiment, the active sites in Dps1 and Dps2 bind only one Fe(II). In Dps1 this site is either 5 or 6 coordinate while in Dps2 this site is definitively 6 coordinate, with weak water ligands probable at the Fe(II) centers in both proteins. The ground state parameters obtained from the VTVH MCD data fitting are analogous suggesting that the geometries of the Fe(II) centers in both proteins are comparable as well. This is consistent with the crystallographic data of Dps1 and Dps2, which show only single metal centers at the supposed ferroxidase sites (Figure 1) (6), therefore we can correlate the single iron binding site identified by CD and MCD studies of Dps1 and Dps2, with the Fe1 sites labeled in Figure 1A and 1B, respectively. As determined by the spectroscopic data, the coordination environment surrounding both single Fe centers is similar. In both crystal structures the iron is ligated by an aspartate, glutamate, and histidine ligand, and a single water (shown by solid bonds in Figure 1A and 1B). The Fe-ligand distances in the Dps1 crystal structure suggest the Fe could be 4-coordinate, although the second oxygen of Asp54 is ~ 2.7 Å from the Fe and may bind in a bidentate mode when Fe(II) is present, explaining the higher coordination number determined from the CD/MCD data. In the Dps2 crystal structure, the terminal aspartate ligand (Asp 56) is well oriented for bidentate coordination which could make this metal center 5-coordinate. Bidentate coordination from the carboxylate (Glu60) seems unlikely; therefore the sixth ligand, required by the CD/MCD data most probably derives from an additional water molecule. One difference between the metal binding sites of the two Dps proteins is the proximity of a large aromatic ring, Phe 20, and an alanine residue at the site in Dps 1 (Figure 1). This more hydrophobic site appears to contain fewer water molecules than the Dps 2 site, and may explain the preference for dioxygen in Dps1, rather than hydrogen peroxide as the oxidant. This could also help account for the 40-fold weaker, Fe(II) binding in Dps1 (Table 1).

The binding of a single Fe(II) at the active sites in both Dps1 and Dps2 mini-ferritins in the absence of oxygen contrasts sharply with some maxi-ferritins. In the case of M-ferritin from amphibians it has been shown that two Fe(II) bind with higher affinity under anaerobic conditions to pre-form a di-ferrous binding site that is able to react with dioxygen (10). Interestingly, in human H-ferritins and some *E. coli* ferritins each active site was also found to preferentially bind one iron center, suggesting a stepwise binding that could be facilitated by dioxygen in these proteins (29,30). In crystal structures of ferritins, and of Dps proteins in particular, the metal ion occupancy of the site is quite varied (5). For example in the Listeria Dps protein crystal structure, in the absence of air and H_2O_2, only a single iron is bound (31), while structures of Dps from *Bacillus brevis* revealed di-metal sites when Hg(II)

or Ag(I) were used (32). Studies on other non-heme iron enzymes show that reduction of O_2 by a mononuclear Fe(II) center is extremely difficult (33,34) and previous kinetic studies of Dps indicated a stoichiometry of two Fe(II) per O_2 or H_2O_2, suggesting that a diiron site is required for reaction with O_2 in Bacillus Dps proteins (3). Thus it seems unlikely that the mononuclear Fe(II) site observed under these anaerobic conditions is reactive, but rather that the oxidant may assist in driving the formation of a binuclear iron site. To assess this model and determine the distribution of mononuclear versus binuclear Fe(II) sites formed in the Dps proteins under anaerobic conditions, speciation curves (Figure 7) were calculated using the binding constants determined from the CD titration data. The results show that a high percentage of mononuclear sites were present below one equivalent of Fe(II) per ferroxidase site, however, only ~5% binuclear sites were present, even well after the addition of two equivalents of Fe(II). Thus, the binding of a single Fe(II) to Dps proteins in the absence of the oxidant indicates that O_2 or H_2O_2 is necessary for completion of the diiron site in mini-ferritins. The role of O_2 or H_2O_2 could be either to shift the equilibrium towards the formation of the binuclear iron site by driving the catalytic reaction or O_2/ H_2O_2 could form a precursor complex with the first iron that would then increase the affinity for the second Fe iron, driving the reaction to completion.

An ordered water appears to pre-form the active site pocket for a second Fe center to bind at the oxidoreductase sites in mini-ferritins, which is labeled in the Dps crystal structures shown in Figure 1. The ordered water is hydrogen bonded to a second histidine ligand near each site (His39 in Dps1 and His41 in Dps2), and is 3.8Å away from the iron center in Dps1 and 4.1 Å away in Dps2. The absence of any other available protein ligands explains the very low affinity (20–40,000 μM, as the minimum estimated K_d), for the second Fe(II) in both Dps proteins. Dioxygen or hydrogen peroxide could bridge the two iron centers in the site, driving its formation and catalysis. It is important to note, however that while Dps2 shows similar reactivity with both dioxygen and hydrogen peroxide, Dps1 shows no reactivity with hydrogen peroxide, and in fact inhibits the solution reaction of hydrogen peroxide with Fe(II). The greater hydrophobicity of the Phe 20 and Ala50 found only at the catalytic site in Dps1 may selectively enhance dioxygen binding while inhibiting H_2O_2 binding in this protein. In either case, inability of H_2O_2 to assist in formation of the diiron site appears to prevent its reactivity. However the strong affinity of the first Fe(II) binding site would decrease Fe(II) in solution, thus inhibiting solution reactions of Fe(II) with peroxide as previously observed in Dps1 (3).

Recognition of single Fe(II) binding to Dps1 and Dps 2 in the absence of the second substrate, dioxygen or hydrogen peroxide, also explains the apparently slower reaction kinetics for mini versus maxi-ferritins, where the specific activity for ferrous oxidation in Dps 1 and 2 appeared to be only ~ 10% that of the maxi-ferritins (3). If, as we deduced from the data in Figures 7 and 8, only ~5% of the possible diiron sites are filled, and diiron sites are required for activity, when we extrapolate the actual specific activity for a Dps protein in which all diiron sites are loaded, the rate would be ~ 2600/sec/mg of protein. The specific activity of maxi-ferritins is ~ 1220 / sec/mg (35). Therefore when the difference in binding affinity and reactions mechanisms are considered, the specific activity of the mini-ferritins and maxi-ferritins are comparable. As we have observed with other non-heme binuclear iron enzymes (33,36), when the di-iron site is formed and accessible to O_2 coordination, O_2 can bridge the diiron site facilitating a two electron transfer. Thus once a di-iron site is formed in either the maxi- or mini-ferritins it is possible that a similar mechanism and therefore activity is observed.

The differences in formation of the binuclear iron sites observed in mini- versus maxi-ferritins – a preformed di-iron site ready to react with dioxygen in maxi-ferritins (10) versus a single bound Fe(II) able to use dioxygen or hydrogen peroxide to drive formation of the

binuclear site in mini-ferritins – may be the result of unique evolutionary origins of mini- and maxi-ferritins, or may be related to the oxidant selectivity, or both. The stable binding of a single Fe(II) at the catalytic site, with H_2O_2 required for binding of the second Fe, provides the advantage of enhanced protein-based Fe(II)/H_2O_2 reactions and minimized solution Fe(II)/H_2O_2 reaction in Dps proteins. In bacteria that contain both maxi-ferritins and Dps proteins, such as *B. anthracis*, Dps proteins confer peroxide resistance that is absent in deletion mutants, while bacterial maxi-ferritins may play a more dominant role in iron storage (5,37–39). Due to the importance of Dps proteins in DNA protection and the preference for H_2O_2 as an oxidant, bacteria increase the synthesis of Dps proteins for peroxide detoxification in response to environmental oxidants, protecting pathogenic bacteria from host production of H_2O_2. The higher affinity Fe(II) sites in maxi-ferritins (10) allow these proteins to function effectively at lower iron concentrations, while Dps proteins can be reserved for moments of high Fe and oxidant concentration when they are most efficient. Binding of the first Fe(II), with H_2O_2 driving formation of the binuclear iron site thereby prevents the formation of hydroxyl radical and blocks Fenton chemistry (2,40) resulting in more effective DNA protection by mini-ferritins when the bacteria is under oxidant stress.

While it is clear that both mini and maxi ferritin reactions result in the synthesis of caged iron oxy biominerals, it is not yet known whether these mechanistic differences may have developed in response to the different biological needs of bacteria versus eukaryotic organisms or simply as a result of separate evolutionary tracks. Further studies are needed to better assess how these unique mechanistic pathways and protein-Fe(II) interactions have evolved within the ferritin family and how they might contribute to differences in function.

Supplementary Material

Refer to Web version on PubMed Central for supplementary material.

Acknowledgments

This research was supported by NSF-Biophysics Program Grant MCB-0919027 (E.I.S.), NIH Hematology Program DK20251 (E.C.T, X.S.L., T.T), Cooley's Anemia Foundation (X.S.L), and JSPS fellowship for research abroad (T.T).

Abbreviations

Dps	DNA Protection during Starvation
LF	ligand field
NIR	near IR
CD	circular dichroism
(VTVH) MCD	(variable-temperature, variable-field) magnetic circular dichroism
ZFS	zero field splitting
J	exchange coupling, coupling between the two iron sites mediated via bridging ligands

References

1. Lewin AC, Moore GR, Le Brun NE. Formation of protein-coated iron minerals. Dalton Trans. 2005; 21:3597–3610. [PubMed: 16258608]

2. Su M, Cavallo S, Stefanini S, Chiancone E, Chasteen ND. The So-Called Listeria innocua Ferritin Is a Dps Protein. Iron Incorporation, Detoxification, and DNA Protection Properties. Biochemistry. 2005; 44:5572–5578. [PubMed: 15823015]

3. Liu X, Kim K, Leighton T, Theil EC. Paired Bacillus anthracis Dps (mini-ferritin) have different reactivities with peroxide. J. Biol. Chem. 2006; 281:27827–27835. [PubMed: 16861227]

4. Castruita M, Saito M, Schottel PC, Elmegreen LA, Myneni S, Steifel EI, Morel FM. Overexpression and characterization of an iron storage and DNA-binding Dps protein from Trichodesmium erythraeum. Appl. Environ. Microbiol. 2006; 72:2918–2924. [PubMed: 16597998]

5. Chiancone E, Ceci P. The multifaceted capacity of Dps proteins to combat bacterial stress conditions: Detoxification of iron and hydrogen peroxide and DNA binding. Biochimica et biophysica acta. 2010; 1800:798–805. [PubMed: 20138126]

6. Elena Papinutto WGD, Pitulis Nea, Battistutta Roberto, Montecucco Cesare, Zanotti Giuseppe. Structure of Two Iron-binding Proteins from Bacillus anthracis. J Biol Chem. 2002; 277:15093–15098. [PubMed: 11836250]

7. Gauss GH, Benas P, Wiedenheft B, Young M, Douglas T, Lawrence CM. Structure of the DPS-Like Protein from Sulfolobus solfataricus Reveals a Bacterioferritin-Like Dimetal Binding Site within a DPS-Like Dodecameric Assembly. Biochemistry. 2006; 45:10815–10827. [PubMed: 16953567]

8. DeLano WL. The Pymol Molecular Graphics System. 2002

9. Solomon EI, Brunold TC, Davis MI, Kemsley JN, Lee SK, Lehnert N, Neese F, Skulan AJ, Yang YS, Zhou J. Geometric and electronic structure/function correlations in non-heme iron enzymes. Chem. Rev. 2000; 100:235–349. [PubMed: 11749238]

10. Schwartz JKL, X S, Tosha T, Theil EC, Solomon EI. Spectroscopic Definition of the Ferroxidase Site in M Ferritin: Comparison of Binuclear Substrate vs Cofactor Active Sites. J. Am. Chem. Soc. 2008; 130:9441–9450. [PubMed: 18576633]

11. Browett WR, Fucaloro AF, Morgan TV, Stephens PJ. Magnetic circular dichroism determination of zero-field splitting in chloro(meso-tetraphenylporphinato)iron(III). J. Am. Chem. Soc. 1983; 105:1868–1872.

12. Ha Y, Shi D, Small GW, Theil EC, Allewell NM. Crystal structure of bullfrog M ferritin at 2.8A resolution: analysis of subunit interactions and the binuclear metal center. J. Biol. Inorg. Chem. 1999; 4:243–256. [PubMed: 10439069]

13. Eerde, Av; Loo, SW-v; Oost, Jvd; Dijkstra, BW. Fortuitous structure determination of ‘as-isolated’ Escherichia coli bacterioferritin in a novel crystal form. Protein Structure Communications. 2006; F62:1061–1066.

14. Elango N, Radhakrishnan R, Froland W, Wallar B, Earhart C, Lipscomb J, Ohlendorf D. Crystal structure of the hydroxylase component of methane monooxygenase from Methylosinus trichosporium OB3b. Prot. Sci. 1997; 6:556–568.

15. Jin S, Kurtz DM, Liu Z-J, Rose J, Wang B-C. X-ray Crystal Structures of Reduced Rubrerythrin and Its Azide Adduct: A Structure-Based Mechanism for a Non-Heme Diiron Peroxidase. J. Am. Chem. Soc. 2002; 124:9845–9855. [PubMed: 12175244]

16. Lindqvist Y, Huang W, Schneider G, Shanklin J. Crystal structure of Delta(9) stearoyl-acyl carrier protein desaturase from castor seed and its relationship to other di-iron proteins. Embo J. 1996; 15:4081–4092. [PubMed: 8861937]

17. Logan D, Su X, Aberg A, Regnstrom K, Hajdu J, Eklund H, Nordlund P. Crystal structure of reduced protein R2 of ribonucleotide reductase: The structural basis for oxygen activation at a dinuclear iron site. Structure. 1996; 4:1053–1064. [PubMed: 8805591]

18. Solomon EI, Pavel EG, Loeb KE, Campochiaro C. Magnetic Circular Dichroism Spectroscopy as a Probe of the Geometric and Electronic Structure of Non-Heme Ferrous Enzymes. Coord. Chem. Rev. 1995; 144:369–460.

19. Straganz GD, Nidetzky B. Reaction coordinate analysis for beta-diketone cleavage by the non-hem Fe(II)=dependent dioxygenase Dke1. J. Am. Chem. Soc. 2005; 127:12306–12314. [PubMed: 16131208]

20. Microcal Software, I. NorthHampton, MA: 1991. Micorcal(TM) Origin, Version 6.0. http://www.microcal.com

21. Zhang Y, Gebhard MS, Solomon EI. Spectroscopic Studies of the Non-Heme Ferric Active Site in Soybean Lipoxygenase: Magnetic Circular Dichroism as a Probe of Electronic and Geometric Structure. Ligand Field Origin of Zero-Field Splitting. J. Am. Chem. Soc. 1991; 113:5162–5175.
22. Pavel E, Kitajima N, Solomon E. Magnetic circular dichroism spectroscopic studies of mononuclear non-heme ferrous model complexes. Correlation of excited- and ground-state electronic structure with geometry. J. Am. Chem. Soc. 1998; 120:3949–3962.
23. Stevens PJ. Magnetic Circular Dichroism. Ann. Rev. Phys. Chem. 1974; 25:201–232.
24. Bennet DE, Johnson MK. Biophys. Acta. 1987; 911:71–80.
25. Neidig ML, Kavana M, Moran GR, Solomon EI. CD and MCD Studies of the Non-Heme Ferrous Active Site in (4-Hydroxyphenyl)pyruvate Dioxygenase: Correlation between Oxygen Activation in the Extradiol and a-KG-Dependent Dioxygenases. J. Am. Chem. Soc. 2004; 126:4486–4487. [PubMed: 15070344]
26. Liu X, Theil EC. Ferritins: Dynamic Management of Biological Iron and Oxygen Chemistry. Acc. Chem. Res. 2005; 38:167–175. [PubMed: 15766235]
27. Bellapadrona G, Stefanini S, Zamparelli C, Theil EC, Chiancone E. Iron translocation into and out of listeria innocua Dps and size distribution of the protein-enclosed nanomineral are modulated by the electrostatic gradient at the three-fold "ferritin-like" pores. J. Biol. Chem. 2009; 284:19101–19109. [PubMed: 19457858]
28. Turano P, Lalli D, Felli IC, Theil EC, Bertini I. NMR reveals pathway for ferric mineral precursors to the central cavity of ferritin. PNAS. 2010; 107:545–550. [PubMed: 20018746]
29. Bou-Abdallah F, Arosio P, Santambrogio P, Yang X, Janus-Chandler C, Chasteen ND. Ferrous ion binding to recombinant human H-chain Ferritin. An isothermal titration calorimetry study. Biochemistry. 2002; 41:11184–11191. [PubMed: 12220183]
30. Bou-Abdallah F, Woodhall MR, Velazquez-Campoy A, Andrews SC, Chasteen ND. Thermodynamic Analysis of Ferrous Ion Binding to *Escherichia coli* Ferritin EcFtnA. Biochem. 2005; 44:13837–13846. [PubMed: 16229472]
31. Ilari A, Latella MC, Ceci P, Ribacchi F, Su M, Giangiacomo L, Stefanini S, Chasteen ND, Chiancone E. The Unusual Intersubunit Ferroxidase Center of Listeria innocua Dps Is Required for Hydrogen Peroxide Detoxification but Not for Iron Uptake. A Study with Site-Specific Mutants. Biochemistry. 2005; 44:5579–5587. [PubMed: 15823016]
32. Ren B, Tibbelin G, Kajino T, Asami O, Ladenstein R. The Multi-layered Structure of Dps with a Novel Di-nuclear Ferroxidase Center. Journal of Molecular Biology. 2003; 329:467–477. [PubMed: 12767829]
33. Wei P, Skulan AJ, Wade H, DeGrado WF, Solomon EI. Spectroscopic and Computational Studies of the de Novo Designed Protein DF2t: Correlation to the Biferrous Active Site of Ribonucleotide Reductase and Factors That Affect O_2 Reactivity. J. Am. Chem. Soc. 2005; 127:16098–16106. [PubMed: 16287296]
34. Davis MI, Wasinger EC, Decker A, Pau MYM, Vaillancourt FH, Bolin JT, Eltis LD, Hedman B, Hodgson KO, Solomon EI. Spectroscopic and Electronic Structure Studies of 2,3-Dihydroxybiphenyl 1,2-Dioxygenase: O_2 Reactivity of the Non-Heme Ferrous Site in Extradiol Dioxygenases. J. Am. Chem. Soc. 2003; 125:11214–11227. [PubMed: 16220940]
35. Liu X, Theil EC. Ferritin Reactions: Direct identification of the site for the diferric peroxide reaction intermediate. Proc. Nat. Acad. USA. 2004; 101:8557–8562.
36. Schwartz JK, Wei P-p, Mitchell KH, Fox BG, Solomon EI. Geometric and Electronic Structure Studies of the Binuclear Nonheme Ferrous Active Site of Toluene-4-monooxygenase: Parallels with Methane Monooxygenase and Insight into the Role of the Effector Proteins in O_2 Activation. J. Am. Chem. Soc. 2008; 130:7098–7109. [PubMed: 18479085]
37. Ishikawa T, Mizunoe Y, Kawabata S, Takade A, Harada M, Wai SN, Yoshida S. The iron-binding protein Dps confers hydrogen peroxide stress resistance to Campylobacter jejuni. J. Bacteriol. 2003; 185:1010–1017. [PubMed: 12533477]
38. Ueshima J, Shoji M, Ratnayake DB, Abe K, Yoshida S, Yamamoto K, Nakayama K. Purification, gene cloning, gene expression, and mutants of Dps from the obligate anaerobe Porphyromonas gingivalis. Infect. Immun. 2003; 71:1170–1178. [PubMed: 12595429]

39. Higuchi M, Yamamoto Y, Kamio Y. Molecular biology of oxygen tolerance in lactic acid bacteria: functions of NADH oxidases and Dpr in oxidative stress. J. Biosci. Bioeng. 2000; 90:484–493. [PubMed: 16232897]

40. Zhao G, Ceci P, Ilari A, Giangiacomo L, Laue TM, Chiancone E, Chasteen ND. Iron and hydrogen peroxide detoxification properties of DNA-binding protein from starved cells. A ferritin-like DNA-binding protein of Escherichia coli. J. Biol. Chem. 2002; 277:27689–27696. [PubMed: 12016214]

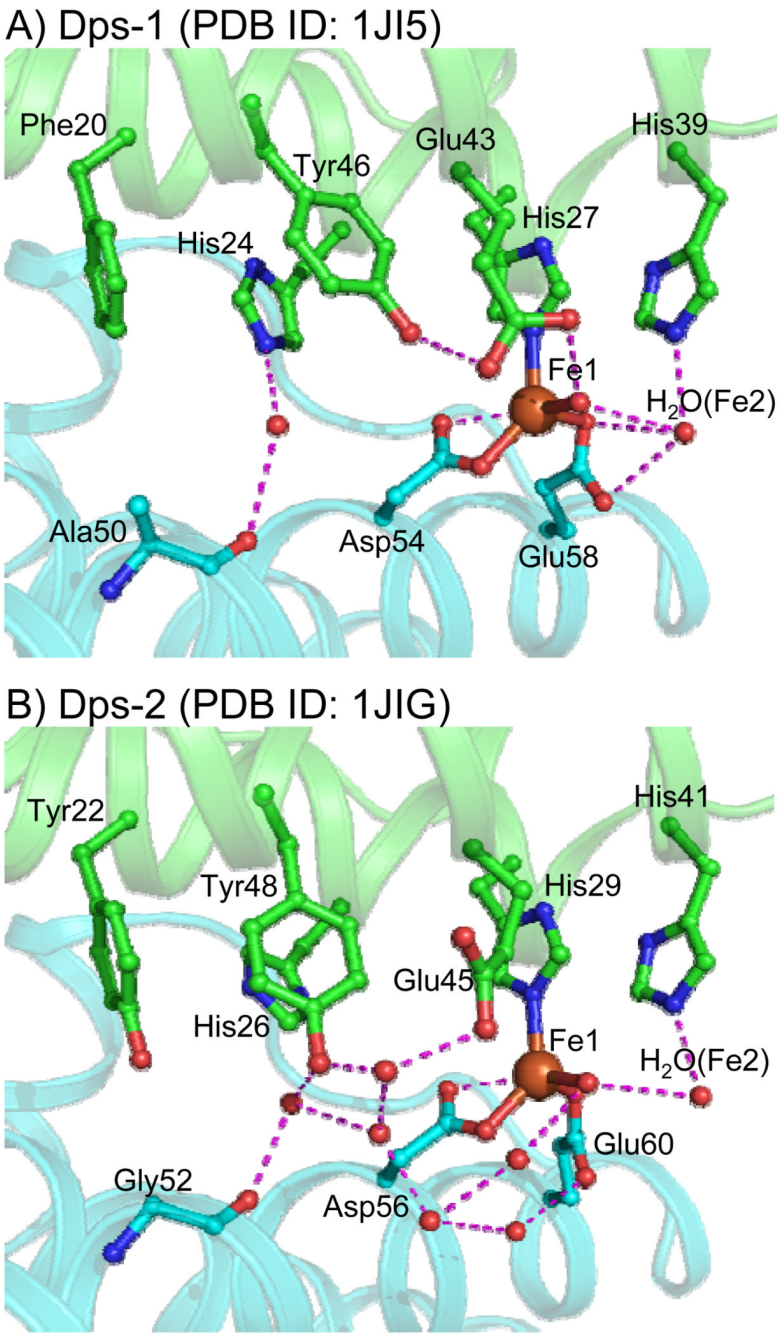

Figure 1.

Representation of intersubunit active sites in (A) Dps1 and (B) Dps 2, obtained from crystal structures 1JI5 and 1JIG, respectively. All protein derived ligands are labeled and water is represented in red. In each structure the water that could occupy the possible second Fe(II) binding site is labeled. In Dps1 this water is 3.8 Å from the first Fe(II) site, and 4.1 Å away in Dps2

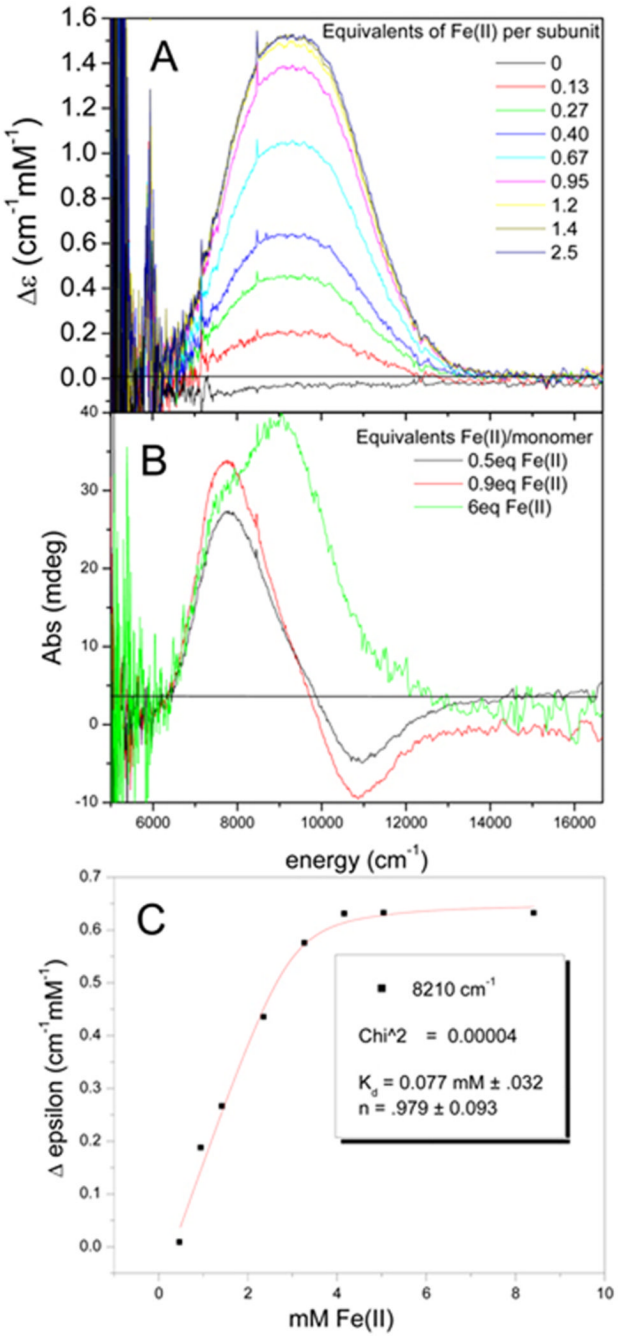

Figure 2.

Anaerobic titration of Dps1 with Fe(II) in (A) CD and (B) MCD. (C) Binding curve with representative intensity for transition at 8300 cm^{-1} plotted against the concentration of Fe(II) added. Fit parameters are given in Table 1.

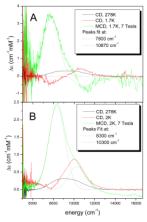

Figure 3.

(A) 278 K CD, 1.7 K CD, and 1.7 K, 7 Tesla MCD spectra of Dps1 with contribution of excess Fe(II) subtracted. Simultaneous peak fitting of these three spectra results in two transitions (gray): at 7800 and 10,870 cm^{-1} (B) Overlay of 278 K CD (black), 2 K CD (red), and 2K, 7 Tesla MCD (green) taken of Dps2. These spectra are best fit with transitions at 8300 and 10300 cm^{-1}

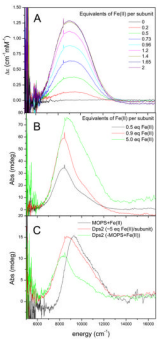

Figure 4.

Anaerobic titration of Dps2 with Fe(II) in (A) CD and (B) MCD. (C) MCD spectra of Fe(II) in a MOPS buffer solution (black), Dps2 with excess Fe(II) (red), and the subtraction spectrum of Dps2 minus Fe(II) in MOPS solution scaled to the appropriate concentration

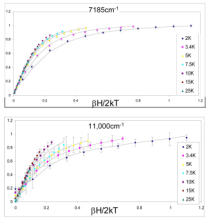

Figure 5.
Fits to VTVH MCD data collected on Dps1 at 7185 and 11000 cm^{-1}, using equation 2.

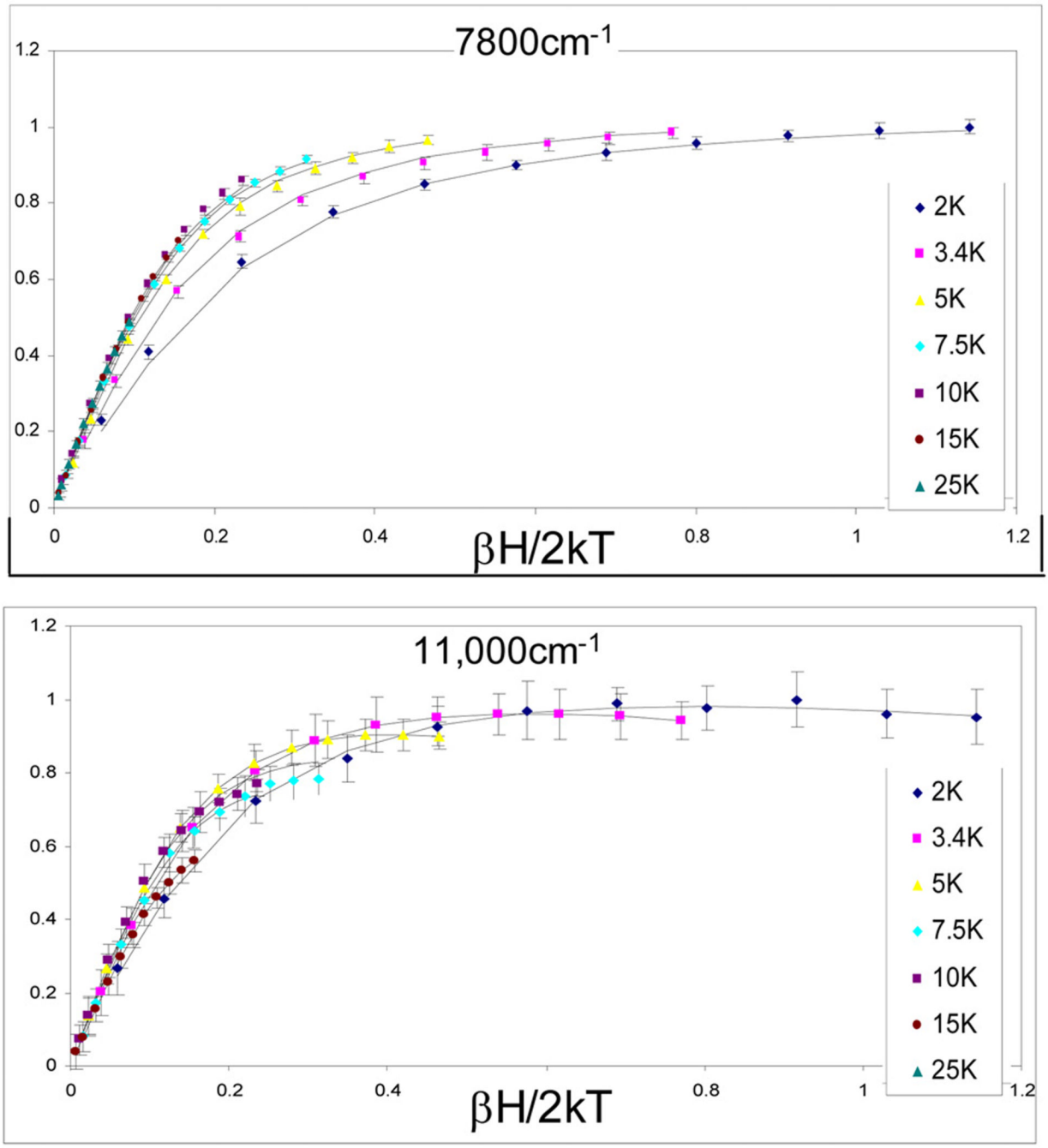

Figure 6.
Fits to VTVH MCD data collected on Dps2 at 7800 and 11000 cm^{-1} using equation 2

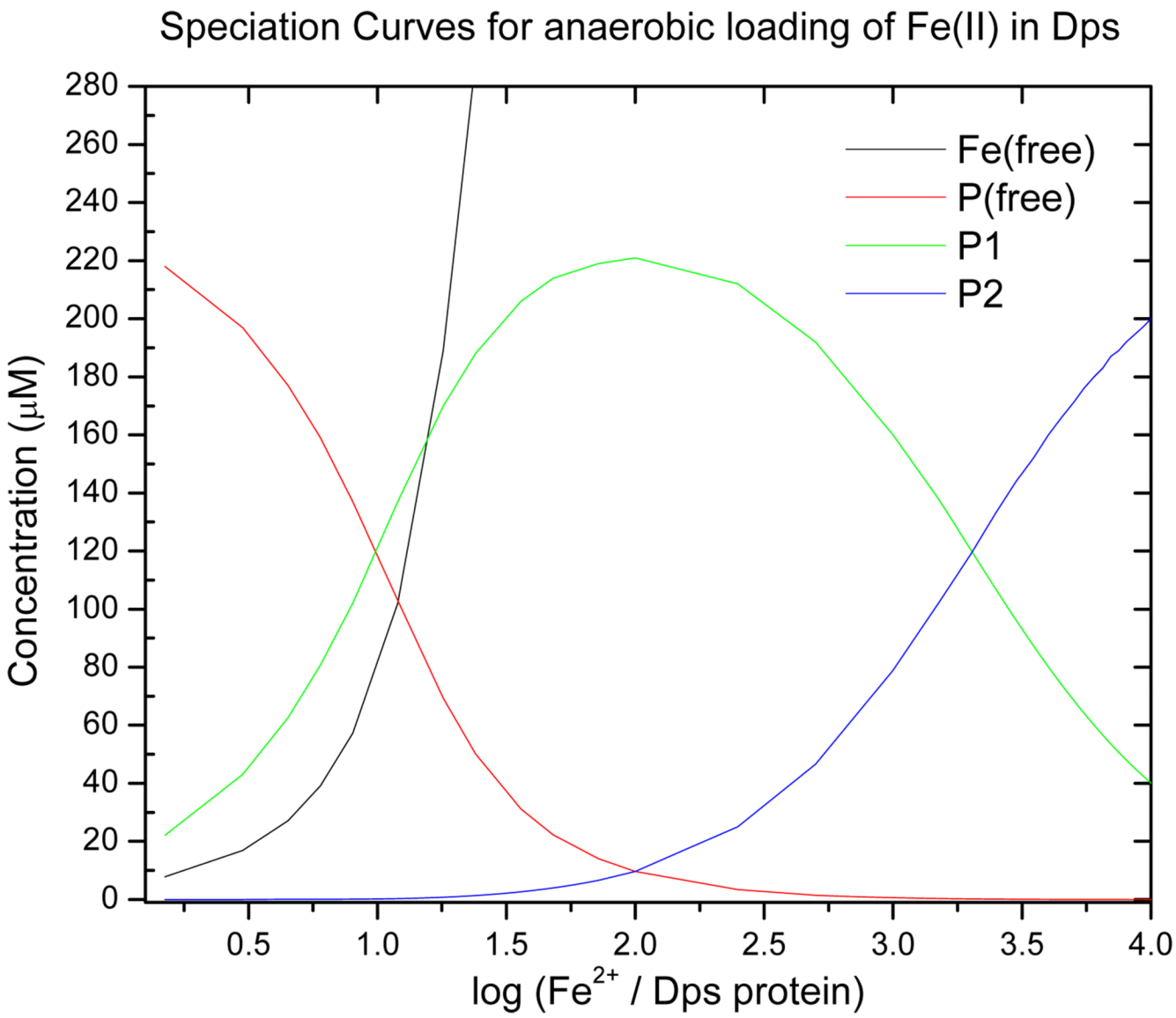

Figure 7.

$[P_f]$, $[P_1]$, $[P_2]$, & $[Fe_f]$ are plotted as a function of $\log([Fe_T] / [P_T])$ from the numerical solution to Equations 3 through 6. Total protein concentration is fixed at 240 μM while total Fe(II) concentration is varied from 0 to 1 M (~4200 Fe^{2+}/Dps). K_{d1} is fixed at 77 μM and K_{d2} is fixed at 40,000 μM. The black line is the concentration of unbound Fe(II) in solution, red is the concentration of empty active sites in the Dps monomers, green is the concentration of mononuclear Fe(II) sites, and blue is the concentration of binuclear Fe(II) sites formed.

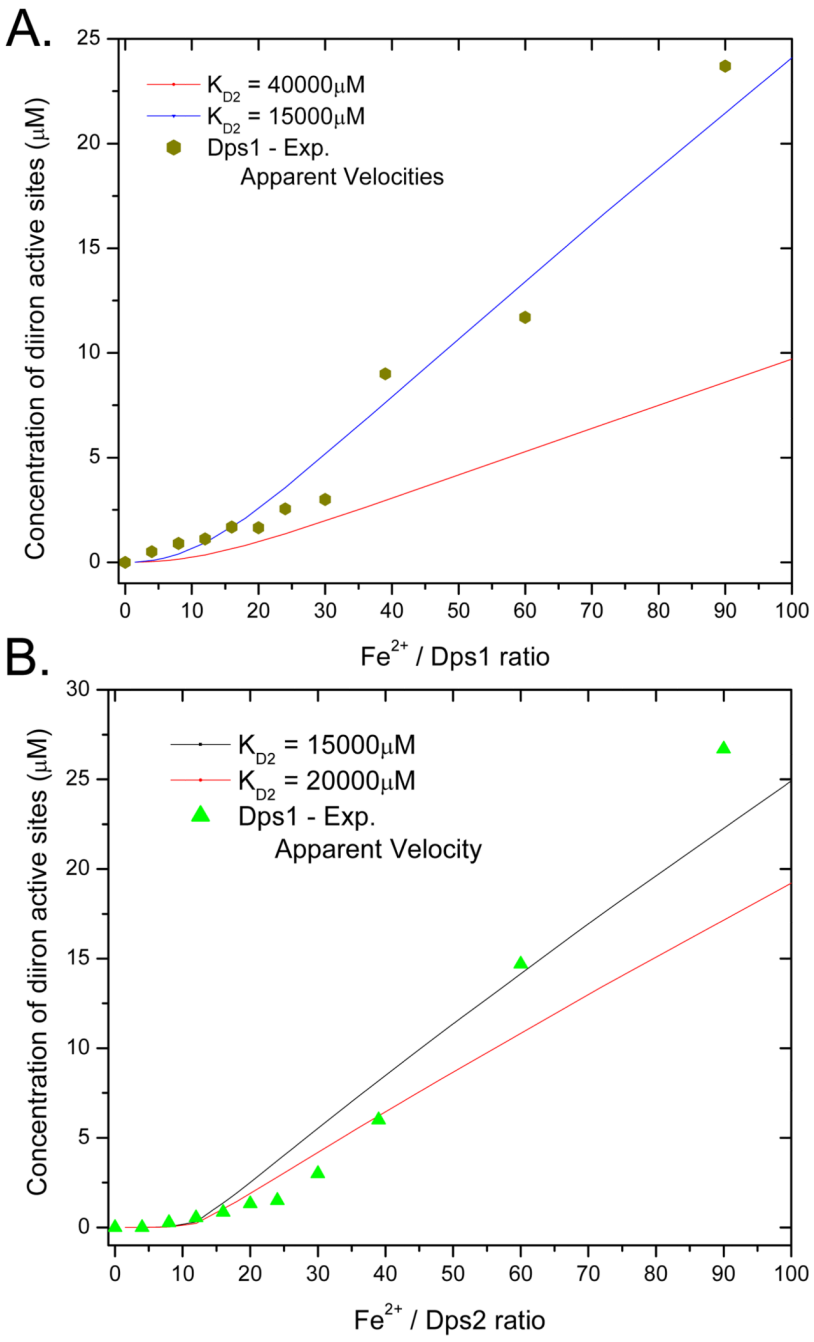

Figure 8.

The apparent initial rates of Fe^{2+} oxidation scaled to overlay with the calculated concentration of binuclear Fe(II) active sites occupied at a given Fe^{2+}/Dps ratio. **A**. Dps 1: The red line is the concentration of binuclear Fe(II) active sites occupied at a given Fe^{2+}/ Dps1 ratio calculated from equations 3 through 6 when K_{D1} is fixed at 77 μM, K_{D2} is fixed at 40,000 μM, and protein concentration is 240 μM. The blue line is the concentration of binuclear Fe(II) active sites occupied when K_{D1} is fixed at 77 μM, and K_{D2} is lowered to 15,000 μM. **B**. Dps2: The red line is the concentration of binuclear Fe(II) active sites occupied when K_{D1} is fixed at 2.1 μM, K_{D2} is fixed at 40,000 μM, and protein

concentration is 240 μM. The blue line is the concentration of binuclear Fe(II) active sites occupied when K_{D1} is fixed at 2.1 μM, and K_{D2} is lowered to 15,000 μM.

Table 1

Properties of Dps 1 and Dps 2 interactions with Fe (II)

	Dps1		Dps2	
		NIR CD		
Transition (cm^{-1})	10300	8600	10300	8100
K_{D1} (μM)	77 ± 32	79 ± 45	2.1 ± 6.8	2.03 ± 3.7
n (number Fe bound)	0.979 ± 0.093	0.841 ± 0.095	1.315 ± 0.025	1.309 ± 0.013
Lower limit for K_{D2} (μM) for Fe2 (computation)	40,000		20,000	